Different types of reactions to E7386 among colorectal cancer patient-derived organoids and corresponding CAFs

TOSHIO IMAI[1,2], MIE NARUSE[1], MASAKO OCHIAI[1], KENJI MATSUMOTO[3], SATSUKI IKEDA[4], MANAMI KANI[4], YUYU KATO[4], AKIYOSHI HIRAYAMA[4], TOMOYOSHI SOGA[4], YUSAKU HORI[5], AKIRA YOKOI[5] and ATSUSHI OCHIAI[2]

[1]Central Animal Division, National Cancer Center Research Institute; [2]Exploratory Oncology Research and Clinical Trial Center, National Cancer Center, Tokyo 104-0045; [3]Department of Allergy and Clinical Immunology, National Research Institute for Child Health and Development, Tokyo 157-8535; [4]Institute for Advanced Biosciences, Keio University, Tsuruoka, Yamagata 997-0035; [5]Oncology Business Group, Eisai Co., Ltd., Tokyo 112-8088, Japan

Received January 28, 2022; Accepted April 27, 2022

DOI: 10.3892/ol.2022.13342

Abstract. Colorectal cancer (CRC) harbors genetic alterations in a component of the Wnt signaling pathway in ~90% of cases. In addition, the Wnt signaling pathway has been previously suggested to serve a notable role in the pathophysiology of CRC cells and cancer-associated fibroblasts (CAFs). In the present study, the possible effects of E7386, a selective inhibitor of the interaction between β-catenin and the cAMP response element-binding protein-binding protein, were evaluated using organoids and the corresponding CAFs derived from patients with CRC. E7386 at 100 nM was revealed to decrease the viability of CRC organoids and CAFs. Analysis of the gene expression profiles revealed marked changes in the expression levels of different types of cancer-associated genes associated with E7386 concentrations in the organoids and/or CAFs, such as those regulating glucose and amino acid metabolism [phosphoenolpyruvate carboxykinase 2, asparagine synthetase (glutamine-hydrolyzing), phosphoserine aminotransferase 1 and phosphoglycerate dehydrogenase], stimulation of natural killer cell-mediated cytotoxicity (UL16-binding protein 1) and modification of the Wnt/β-catenin signaling pathway (indicated by very low density lipoprotein receptor). Results of the hydrophilic metabolome analysis in the organoids were consistent with those of the transcriptomic analysis. *In vivo* experiments used corresponding xenograft models, although changes in volume of tumor tissues could not be observed at 50 mg/kg body weight twice a day for 14 days, results on the protein expression levels partially supported those in the *in vitro* experiments. In conclusion, different types of reactions, such as alterations in the glucose and amino acid metabolic pathways, stimulation of stress responses and NK-cell mediated cytotoxicity and components in the Wnt/β-catenin signaling pathway, to E7386 in the CRC organoids and corresponding CAFs were observed under conditions with decreased cell viability. However, further mechanistic studies to clarify the relationships with Wnt/β-catenin signaling pathway and these reactions using preclinical models and biomarker studies using clinical human samples are required for verification of the present preclinical biomarkers.

Correspondence to: Dr Toshio Imai, Central Animal Division, National Cancer Center Research Institute, 5-1-1 Tsukiji, Chuo-ku, Tokyo 104-0045, Japan
E-mail: toimai@ncc.go.jp

Key words: colorectal cancer, organoids, cancer-associated fibroblasts, patient-derived xenograft, E7386

Introduction

Colorectal cancer (CRC) is the fourth most common human malignancy, with ~900,000 cases of mortality worldwide annually (1). In addition, it is the second most common cause of cancer-associated mortality in the United States (2). Regarding the molecular mechanism underlying CRC carcinogenesis, a model was previously proposed, where the steps required for its development involve the activating mutation of *KRAS* combined with the inactivating mutations of tumor suppressor genes, such as *adenomatous polyposis coli* (*APC*), *SMAD4* and *TP53* (3). When devising strategies for developing molecular target-based drugs, intertumoral and intratumoral genetic heterogeneity are garnering research interest due to their key role in cancer evolution (4), in which CRC is of no exception (5). CRC has been reported to harbor genetic alterations in components of the Wnt signaling pathway in ~90% of the cases (6,7). Furthermore, the Wnt signaling pathway has been reported to serve a key role in the activation of not only CRC cells but also cancer-associated fibroblasts (CAFs) (8). Models of organoids and CAFs (9), in addition to those of patient-derived xenografts (PDX), were previously established using surgical specimens isolated from each corresponding patient. This was conducted in parallel with the targeted sequencing of cancer-associated gene mutations to

evaluate efficacy of anticancer drugs to individual patient in a partially-reproduced tumor microenvironment.

E7386 is a selective inhibitor of the interaction between β-catenin and the cAMP response element binding protein-binding protein, which forms a part of the Wnt/β-catenin signaling pathway (10). Therefore, E7386 is expected to affect CRC cells, particularly those with aberrant activation of the Wnt/β-catenin signaling pathway. In the present study, the effects of E7386 treatment on the *in vitro* models of CRC-derived organoids and a co-culture model of these organoids with corresponding CAFs were comprehensively analyzed on a molecular level. Subsequently, the effects of E7386 on the *in vivo* PDX model were also investigated, to screen for potential pharmacodynamic biomarkers that are applicable for clinical trials. In addition, the pharmacological effects of E7386 were examined.

Materials and methods

Chemicals. A stock solution of E7386 dissolved in DMSO to 10 mM and E7386 powder (Eisai Co., Ltd.) diluted with 100 mM hydrochloric acid was used for *in vitro* and *in vivo* studies, respectively.

Surgical tissue specimens. A total of 45 surgical CRC specimens collected after the pathological examination of patients with CRC at the National Cancer Center Hospital (Tokyo, Japan) were received between February 2016 and February 2018 and used to prepare organoids/fibroblast culture and implantation into mice for the establishment of PDX. Of the 45 cancer patients, 60% were males and 40% were females, and average ages were 62 years old, ranging from 36 years old to 88 years old. All experiments were performed following the relevant domestic guidelines and regulations in Japan, including Ethical Guidelines for Medical and Health Research Involving Human Subjects. The use of surgical specimens in this study was approved by the Ethics Committee of the National Cancer Center (approval no. 2015-108) and written informed consent was obtained from all patients. In the present study, three cases of typical gene mutational statuses [case 21: *KRAS*, *APC* and *TP53*; case 28: *PI3K catalytic subunit* (*PIK3CA*) and *TP53*; and case 32: *APC* and *TP53*] were used (9). Clinical and pathological information has been previously reported (9).

Culture of organoids and fibroblasts and co-culture of organoids with fibroblasts using a chamber system. The organoids and fibroblasts used in the present study were established from surgical specimens. The culturing of organoids and fibroblasts was performed as previously described (9). Briefly, for co-culture, organoids and fibroblasts were cultured in inserts with porous membranes and carrier plates (pore size, 1 μm; cat. nos. 353104 and 353504; Corning, Inc.). In total, 1 day before co-culture, fibroblasts ($1x10^4$ cells/well) were seeded into 24-well plates with RPMI-1640 (cat. no. 189-02025; Fujifilm Wako Pure chemical Corporation) containing 10% FBS (cat. no. SH30075; Hyclone; Cytiva). Organoids ($1x10^4$ cells/insert) were seeded into polymerized Matrigel (cat. no. 354234; Corning, Inc.) in cell culture inserts, followed by setting the inserts in companion carrier plates, and a medium for organoid culture was added into the basal compartments. The next day, the organoids were covered with Matrigel, and the inserts containing the organoids were transferred to the 24-well plates containing the fibroblasts. During co-culturing, the organoid culture medium was applied to both organoids and fibroblasts. After E7386 incubation for 6 or 24 h, organoids and fibroblasts in each insert and well were collected separately for the analysis of gene expression.

Establishment of the PDX model. Surgical specimens were cut 2 or 3-mm cubes or established CRC organoids were implanted into the subcutis of female NOD.Cg-*Prkdc*^{scid}*Il2rg*^{tm1Sug}/ShiJic (NOG) mice at 7 weeks of age (In-Vivo Science, Inc.) under isoflurane anesthesia (4% for initiation and 2% for maintenance), and their body weights were 20.8±0.8 g at 14-16 weeks of age (at the start of drug administration). The mice were housed in plastic cages (n≤5 per cage) with recycled paper bedding in a specific-pathogen-free environment maintained at 22±1˚C and 55±10% relative humidity, with 12-h light/dark cycle and were provided free access to the CE2 standard chow diet (CLEA Japan, Inc.) and tap water. Mouse experiments were performed at the Animal Facility of the National Cancer Center Research Institute (Tokyo, Japan) according to institutional guidelines. Ethics approval was obtained from the National Cancer Center Animal Ethics Committee (approval no. T17-006).

Treatment of E7386 in the in vitro and in vivo systems. For the *in vitro* studies, E7386 at concentrations of 0, 10, 30, 100 and 300 nM in culture media was used, before cell viability was measured using the RealTime-Glo™ MT Cell Viability Assay solution kit (cat. no. G9711; Promega Corporation). Organoids/CAF samples planned for RNA analysis were collected 6 and 24 h after treatment, whereas those planned for metabolome analysis were collected 24 h after the addition of E7386. Triplicate samples of organoids and corresponding CAFs from each case were used for the measurement of cell viability.

For the *in vivo* PDX mouse model, E7386 solution was administered at 0 and 50 mg/kg body weight by gavage twice a day for 14 days. The number of mice used in the experiments were five of case 21, five of case 28 and three of case 32 per the control and E7386-treated group each. The size of the implanted tissue was measured using a caliper. In total, 6 h after the last drug administration, all mice were sacrificed by cervical dislocation under 4% isoflurane anesthesia before subcutaneous PDX tissues were excised cut into pieces, frozen and stored at -80˚C or fixed with 10% neutral buffer formalin.

Gene expression analyses for in vitro experiments using DNA microarrays and reverse transcription-quantitative PCR (RT-qPCR). Total RNA was isolated using the RNeasy Micro Kit (cat. no. 74104; Qiagen GmbH). Triplicate samples were prepared for the RNA cocktail used for DNA microarray analysis from E7386-0, 30, and 100 nM groups. The quality of RNA samples and DNA microarray analysis [SurePrint G3 Human GE Microarray GE 8x60 K Ver.3.0 (cat. no. G4851C; Agilent Technologies, Inc.)] were evaluated as previously described (9). For RT-qPCR analysis, aliquots of total RNA were subjected to a reverse transcription with random primers using the High-Capacity cDNA Reverse Transcription Kit (cat. no. 4368814; Applied Biosystems; Thermo Fisher

Scientific, Inc.). qPCR in duplicate in three independent experiments was performed using the SsoAdvanced™ Universal SYBR-Green Supermix (cat. no. 172-5271; Bio-Rad Laboratories, Inc.) in the DNA Engine Opticon® 2 system (MJ Research, Inc.; Bio-Rad Laboratories, Inc.). The primer sequences are shown in Table SI. Data were normalized to the housekeeping gene *β-actin*, calculated using the $2^{-\Delta\Delta Cq}$ method (11) and are presented as the mean ± standard deviation (1.0-fold was as control).

Gene ontology (GO) enrichment analysis. To clarify the biological meaning of the key molecules, gene information obtained in the DNA microarray analysis was loaded into Metascape 3.5 (https://metascape.org) for GO enrichment analysis (12). Terms with a P<0.01, ≥3 and an enrichment factor >1.5 were collected before being grouped into clusters based on their membership similarity (κ-score >0.3).

Hydrophilic metabolome analysis of the in vitro data. For hydrophilic metabolite analysis, capillary electrophoresis time-of-flight mass spectrometry (CE-TOFMS) was used for cationic and anionic metabolite analyses. To extract the metabolites, cultured organoids from E7386-0, 30, and 100 nM groups were collected after adding 1.0 ml methanol containing internal standards (25 μM each of methionine sulfone and D-camphor-10-sulfonic acid). The suspension (400 μl) was then mixed with Milli-Q water and chloroform at a volumetric ratio of 5:2:5 and centrifuged at 9,100 x g for 10 min at 20˚C. Subsequently, the aqueous layer (400 μl) was centrifugally filtered through a 5 kDa cut-off filter (cat. no. UFC3LCCNB-HMT; Human Metabolome Technologies, Inc.) to remove proteins. The filtrate was centrifugally concentrated and dissolved in 25 μl Milli-Q water containing the reference compounds (200 μM each of 3-aminopyrrolidine and trimesic acid) immediately prior to CE-TOFMS analysis [Agilent 1100 isocratic HPLC pump, Agilent G1603ACE-MS adapter kit, and Agilent G1607A CE-electrospray ionization (ESI)-MS sprayer; Agilent Technologies, Inc.] (13,14). The quantified data were standardized with the internal standards before being normalized to the DNA concentrations of each sample.

Histopathological and immunohistochemical analyses of in vivo experiments. PDX tissues fixed with formalin were routinely processed into paraffin-embedded (FFPE) sections and stained with hematoxylin and eosin for histopathological evaluation using a transmission light microscope (BX51; Olympus Corporation).

Immunohistochemistry was performed using the FFPE sections and primary antibodies against β-catenin (cat. no. 610154; clone 14; BD Biosciences), phosphoenolpyruvate carboxykinase 2 (PCK2; (cat. no. 14892-1-AP; ProteinTech Group, Inc.), α-smooth muscle actin (αSMA; cat. no. M0851; clone 1A4; Agilent Technologies, Inc.) and very low density lipoprotein receptor (VLDLR; cat. no. ab203271; Abcam). Antigen retrieval was performed by autoclaving at 121˚C for 10 min in citric acid buffer (pH 6.0) or proteinase K (FUJIFILM Wako Pure Chemical Corporation) treatment. For signal detection, Histofine MAX PO solution (cat. no. 424131; Nichirei Corporation) was applied, visualized with 3,3'-diaminobenzidine followed by counterstaining with hematoxylin. Negative controls without primary antibody addition was set for each antigen. Quantitative imaging analysis of αSMA-positive areas was performed using the HALO Imaging Analysis Platform (001-WS-HALO; Indica Labs, Inc.).

For the immunoblotting of β-catenin and PCK2, protein samples (10 μg) extracted with RIPA Lysis kit (cat. no. WSE-7420; ATTO Corporation) from the PDX tissues were subjected to SDS-PAGE. Immunoblotting and detection of chemiluminescence signals (cat. no. WSE-7120; ATTO Corporation) were performed as previously reported (15). Quantitative analysis was performed using Science Lab. 2005, Multi Gauge Ver. 3.0 software (FUJIFILM Wako Pure Chemical Corporation). For the internal control, a primary antibody against β-actin (cat. no. A1978; clone AC-15; Sigma-Aldrich; Merck KGaA) was used.

Statistical analysis. Quantitative data from *in vitro* and *in vivo* experiments, including cell viability assay, hydrophilic metabolomics, RT-qPCR and immunoblotting analysis results were presented as the mean ± SD. Homogeneity of variance in data was checked by Bartlett's test. When the data were homogenous, differences among the control and treatment groups were analyzed by one-way analysis of variance (ANOVA) or two-way ANOVA followed by Tukey's test using Easy R (EZR ver. 4.1.2) (16). In the heterogenous cases, Kruskal-Wallis test followed by Bonferroni test was applied. Immunohistochemical grade data were tested using Fisher's exact test in EZR. P-values of <0.05 were considered significant.

Results

Effects of E7386 on the viability of CRC organoids and CAFs varies among the cases. In total, three types of organoids, each harboring the following gene mutational status, were prepared (Fig. 1): i) *APC*, *KRAS* and *TP53* mutations (case 21); ii) *APC* and *TP53* mutations (case 32); or iii) *PIK3CA* and *TP53* mutations (case 28). After comparison with the baseline cell viability of organoids or CAF monoculture in the E7386 (0 nM) group, cell viability was found to vary among the cases dependent on their origin. Increased cell viability of organoids following co-culture with CAFs was observed in cases 21 (P<0.05) and 32 (P<0.01) but not in case 28, which was reported previously (9). By contrast, an inhibitory effect of E7386 at 100 nM on the organoids from cases 21 and 32 was observed, which was more potent in the co-cultured groups (P<0.01). However, these inhibitory effects were diminished in the single-cultured groups from case 21 at 100 nM E7386. In case 28, inhibitory effects of E7386 on the organoids were observed in the co-culture group at 300 nM (P<0.05). In terms of CAFs, potentiating effects of co-culturing with organoids on viability were observed in case 28 (P<0.01) but not in cases 21 and 32. However, the degree of this enhancement was smaller compared with that in the organoids. Inhibitory effects of E7386 on the CAFs could be found at 100 nM, which was more potent in the single-culture groups from all three cases (P<0.01). There were slight differences in the sensitivity of the CAFs to E7386 among the co-cultured groups.

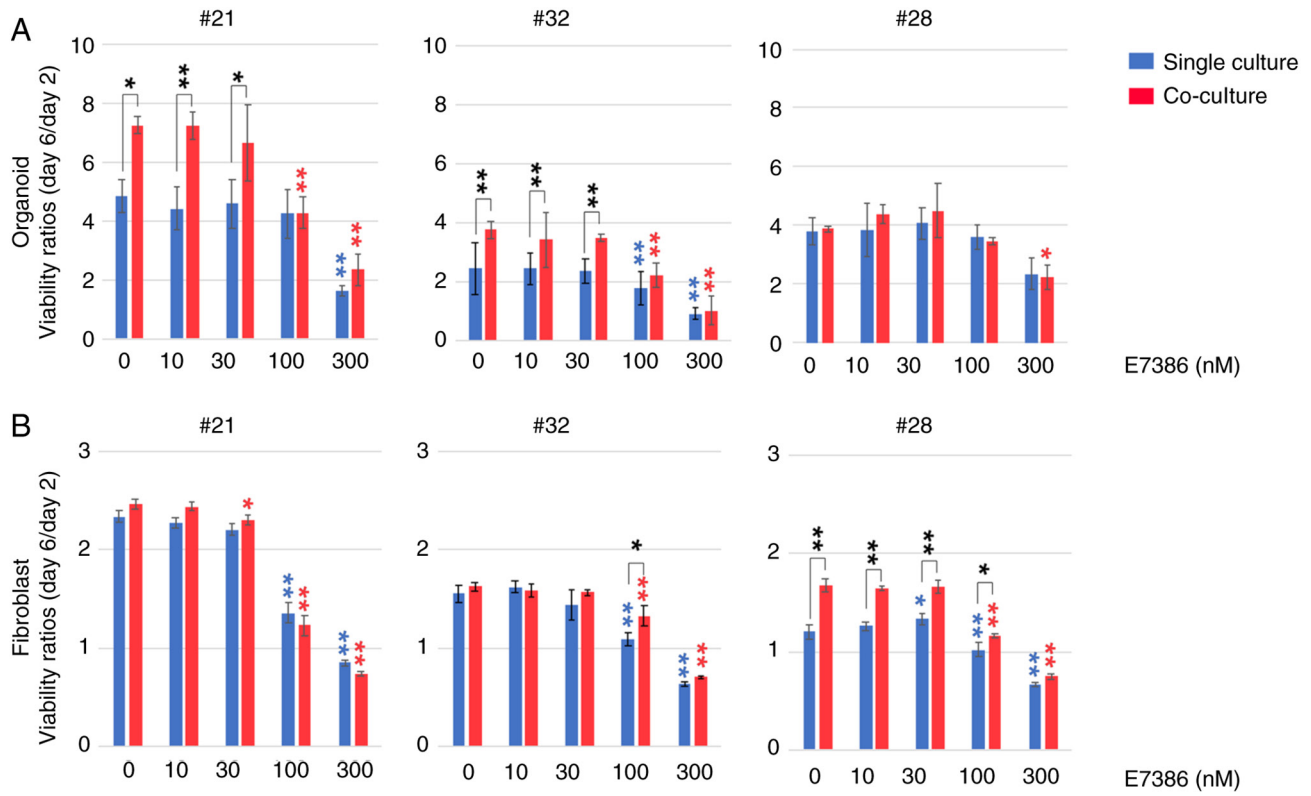

Figure 1. Viability of CRC organoids and CAFs. (A) Viability of the monoculture colorectal cancer organoids and those co-cultured with CAFs 96 h after the addition of E7386. (B) Viability of the CAF monoculture and those co-cultured with organoids 96 h after the addition of E7386. The cell viability data represent relative fold-changes to those at the start of E7386 treatment. *P<0.05 and **P<0.01. The color of asterisks represents significance compared to the corresponding 0 nM controls in single culture (blue) or co-culture (red) groups. CRC, colorectal cancer; CAFs, cancer-associate fibroblasts.

Changes in the expression of genes regulating stress responses and cellular metabolism after E7386 treatment in CRC organoids and/or CAFs. The effects of E7386 on gene expression in the organoids and CAFs were next evaluated using DNA microarrays. In the organoids, 46 genes were found to be upregulated associated with E7386 concentration (correlation coefficient >0.7) 24 h after E7386 treatment (Table SII). GO term enrichment analysis of these upregulated genes revealed that genes associated with stimulation, such as *glutathione-specific γ-glutamylcyclotransferase 1* (*CHAC1*) and *growth factor receptor bound protein 10* (*GRB10*), in addition to those associated with trans-sulfuration and one-carbon metabolism, including *phosphoserine aminotransferase 1* (*PSAT1*), *cystathionine γ-lyase* and *phosphoglycerate dehydrogenase* (*PHGDH*), were amongst the most significantly enriched genes (Fig. S1A). In addition, *UL16-binding protein* (*ULBP*)*1*, which enhances susceptibility to natural killer (NK)-cell-mediated lysis of cancer cells (17) and *PCK2*, which regulates metabolic adaptation and enables glucose-independent tumor growth (18), were included amongst the upregulated genes. A number of the upregulated genes associated with E7386 concentrations were also categorized as ≥ two increased genes with significance (P<0.05) at 100 nM E7386, but associations between the gene expression changes and inhibition of the viability of CRC organoids by E7386 were uncertain (Figs. S2A and S3A). Among the genes that were significantly decreased by two-fold at 100 nM E7386, the cancer-related genes were not enriched (data not shown). RT-qPCR analysis was subsequently performed for *CHAC1*, *ULBP1* and *PCK2* to verify the results from the DNA microarray analysis. Elevated expression (P<0.01) of the three genes was observed in the single-culture organoids and after they were co-cultured with CAFs in the three cases (Fig. 2A). As a transport of small molecule-related genes (Fig. S1A), *VLDLR* expression was also found to be upregulated in association with E7386 concentrations according to results from DNA microarrays, which was confirmed by RT-qPCR in both single-culture organoids and co-cultures consisting of organoids and CAFs from case 32 but cases 21 and 28 (data not shown). The expression of 17 genes were downregulated associated with E7386 concentrations according DNA microarrays in the organoids following E7386 treatment (Table SIII). The results from the GO term enrichment analysis are shown in Fig. S1B. The downregulated genes included *GRPEL1*, *histone deacetylase 2* (*HDAC2*) and *farnesyl diphosphate synthase* (*FDPS*). For the expression of *FDPS* and *HDAC2*, RT-qPCR analysis was performed to verify the results from the DNA microarray. No clear changes in *FDPS* expression could be found, whereas a trend toward a reduction in *HDAC2* expression was observed in the organoids co-cultured with CAFs from cases 32 and 28 (Fig. 2B). For *HDAC* and *FDPS* expression, suggestive relationships with the Wnt/β-catenin signaling pathway were introduced (19,20).

In the corresponding CAFs for each organoid, 52 upregulated and 21 downregulated genes related to E7386 concentrations (correlation coefficient >0.9 and <-0.9, respectively) were found 24 h after the addition of E7386 (Tables SIV and SV). After they were evaluated at correlation coefficients

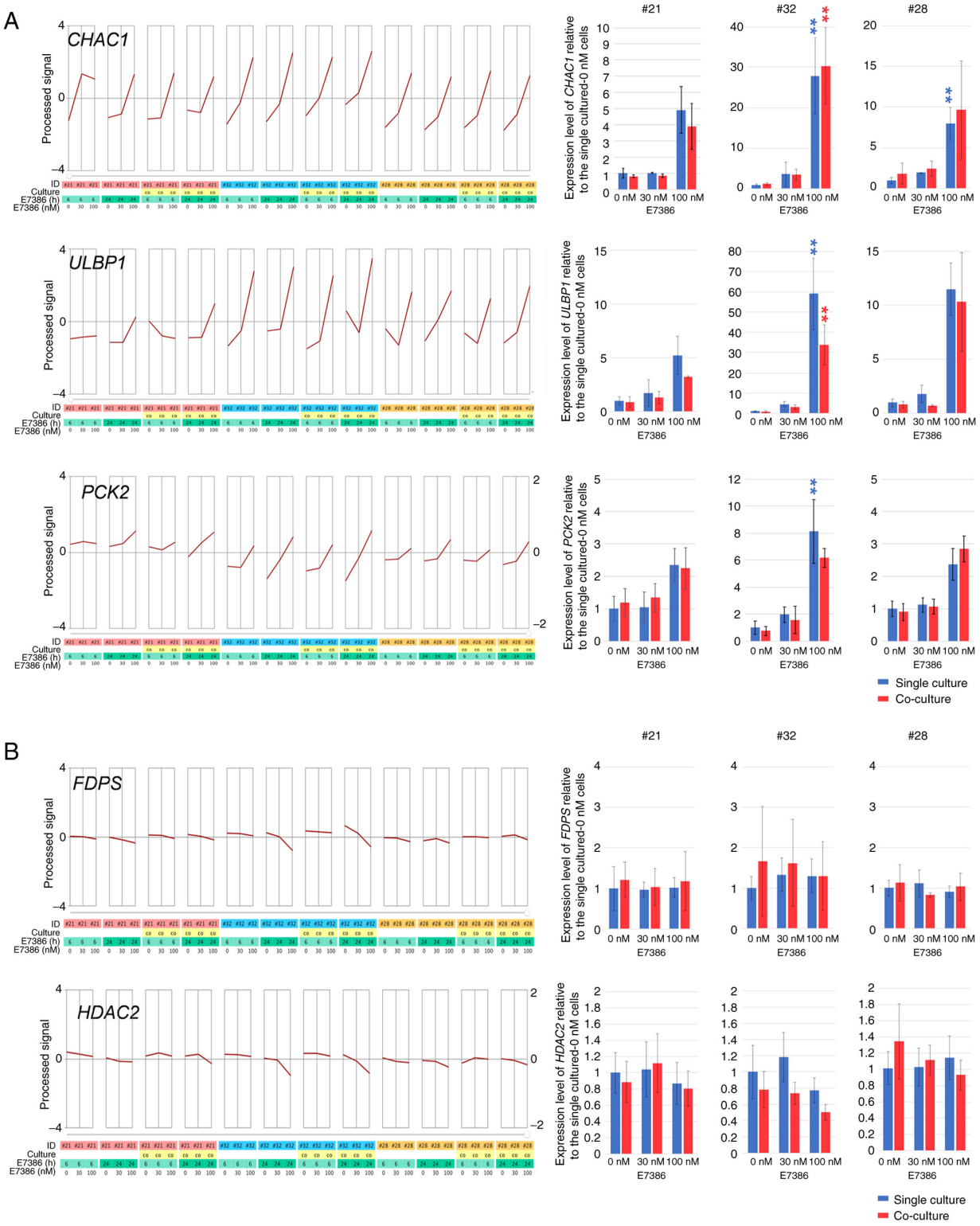

Figure 2. Changes in the expression of genes regulating stress responses and cellular metabolism after E7386 treatment in CRC organoids. (A) Upregulation of *CHAC1*, *ULBP1* and *PCK2* expression associated with E7386 concentration 24 h after the addition of E7386 in CRC organoids. (B) Downregulation of *FDPS* and *HDAC2* expression associated with E7386 concentration 24 h after the addition of E7386 in CRC organoids. Results were obtained using DNA microarray (correlation coefficient >0.7; left) and reverse transcription-quantitative PCR (right). Data are presented as the mean ± SD. **P<0.01. The color of asterisks represents significance compared to the corresponding 0 nM controls in single culture (blue) or co-culture (red) groups. CRC, colorectal cancer. CHAC1, glutathione-specific γ-glutamylcyclotransferase 1; ULBP1, UL16 binding protein 1; PCK2, phosphoenolpyruvate carboxykinase 2; FDPS, farnesyl diphosphate synthase; HDAC2, histone deacetylase 2.

of >0.7 and <-0.7, 458 upregulated and 431 downregulated genes were found (data not shown). GO term enrichment analysis of the upregulated genes revealed that those associated with cellular amino acid metabolism, including *asparagine synthetase* (*glutamine-hydrolyzing; ASNS*), *PSAT1*, *PHGDH* and *glycyl-tRNA synthetase 1* (*GARS*), were amongst the most

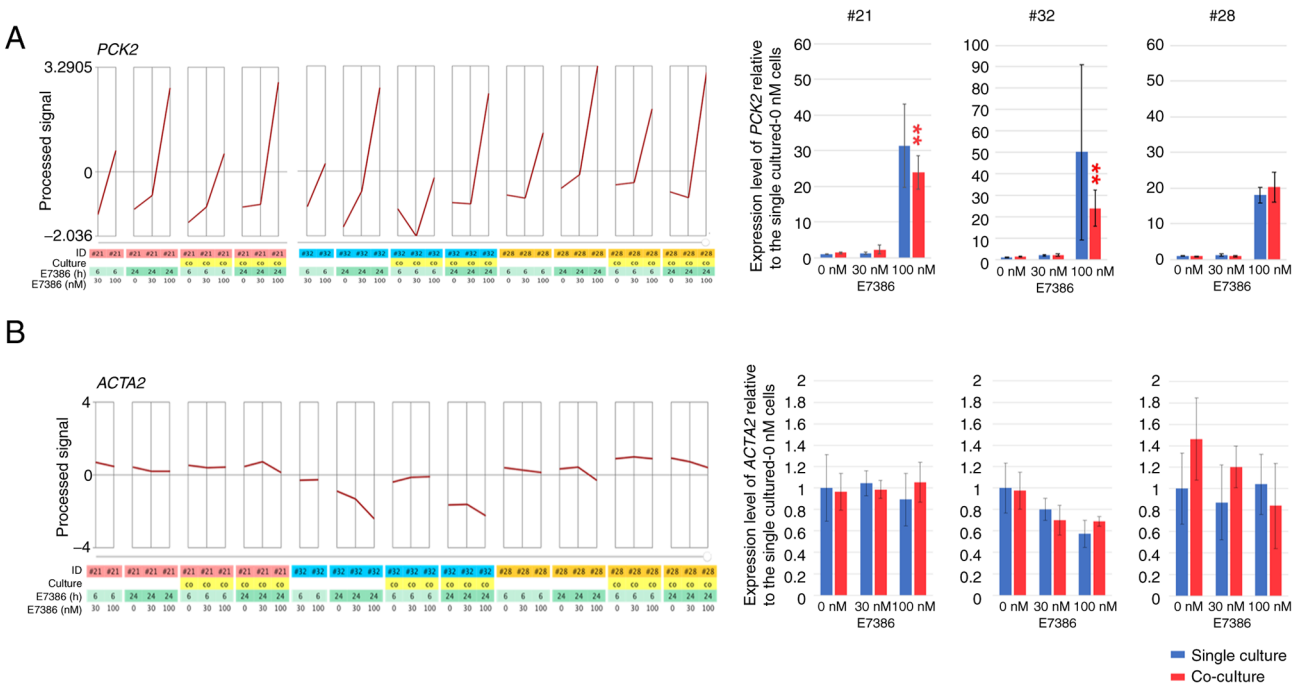

Figure 3. Changes in the expression of genes regulating cellular metabolism and associated with cellular activated status after E7386 treatment in CAFs. (A) Upregulation of *PCK2* expression tied to E7386 concentration (correlation coefficient >0.7) 24 h after the addition of E7386 to the cancer-associated fibroblasts. (B) Downregulation of *ACTA2* expression 6 and 24 h after the addition of E7386 to the organoids from cases 32 and 28. Results were obtained using DNA microarray (correlation coefficient >0.7; left) and reverse transcription-quantitative PCR (right). Data are presented as the mean ± SD. **P<0.01. The color of asterisks represents significance compared to the corresponding 0 nM controls in single culture (blue) or co-culture (red) groups. PCK2, phosphoenolpyruvate carboxykinase 2; ACTA2, smooth muscle actin α2; CAF, cancer-associated fibroblasts

significantly enriched genes (Fig. S1C). In addition, those associated with gluconeogenesis, such as *PCK2*, *activating transcription factor 4* and *sestrin 2*, were upregulated in the E7386-treated CAFs. Various upregulated genes related to E7386 concentrations were also categorized as ≥ two increased genes with a significance of P<0.05 at 100 nM E7386, but associations between the gene expression changes and inhibition of the viability of CAFs by E7386 were uncertain (Figs. S2B and S3B). Among these genes associated with glucose and amino acid metabolism, *ASNS*, *PSAT1*, *PHGDH* and *PCK2* expression were also increased in the organoids. The genes downregulated associated with E7386 concentrations included those associated with the resolution of sister chromatid cohesion, such as *centromere protein O*, *spindle pole body component 25* and *structural maintenance of chromosomes 1A* (Fig. S1D). In total, ≥ two decreased genes with significance at 100 nM E7386 included those involved in mitotic cell cycle processes, such as cyclin *E1* and *MYBL2* and in DNA replication, such as *ATPase family AAA domain-containing 5* and *zinc finger GRF-type-containing 1* (Fig. S3B). Upregulation of PCK2 (P<0.01) expression was then confirmed by RT-qPCR in the single-culture CAFs and in the co-culture with organoids in each case (Fig. 3A). As a gene decreased by E7386, *diaphanous related formin 1* (*DIAPH1*) was reported to be associated with the differentiation of hepatic stellate cells into tumor-promoting myofibroblasts (21). Therefore, to evaluate the alterations in the general activity of CAFs, the expression levels of *ACTA2*, which is a classical gene associated with an activated status of fibroblasts (8), were examined. They were found to be partially downregulated in cases 32 and 28 (Fig. 3B).

Depletion of glycolysis-associated metabolites by E7386 treatment in the CRC organoids. The quantified levels of metabolites produced by the pentose phosphate pathway, glycolysis, tricarboxylic acid (TCA) cycle, amino acid metabolism and their derivatives were obtained from the organoid samples in triplicate after treatment with E7386 for 24 h. The data are presented graphically on a large-scale metabolomic map (Fig. S4) and summarized in Fig. 4. The concentrations of glucose-6-phosphate (G6P) and glucose-1-phosphate (G1P) in the control (0 nM E7386) of case 21 were higher compared with those of cases 32 and 28 (P≤<0.05). In addition, G6P and G1P levels in case 21 were reduced by E7386 treatment (P≤<0.001), but those of cases 32 and 28 were unchanged, suggestive of E7386-induced glucose depletion in case 21. As a response to this effect, gluconeogenesis followed by the reduced levels of metabolites in the TCA cycle was observed in organoids from case 21. In terms of amino acids, the majority of essential amino acids, including histidine, isoleucine, leucine, methionine, phenylalanine, threonine, tryptophan and valine, in addition to a number of nonessential amino acids, including alanine and glutamate, were found to be at higher levels in the control conditions from case 21 compared with those from cases 32 and 28. Furthermore, those of case 21 were reduced by E7386 treatment (Fig. S4).

Changes in the expression levels of PCK2 and VLDLR in carcinoma cells and α-SMA in CAFs are partly verified in the PDX models. PDX using samples from case 21 was successfully established, whereas organoids from case 28, which were engrafted and passaged in the subcutis of NOG mice, were used as PDXs. For case 32, organoids implanted into

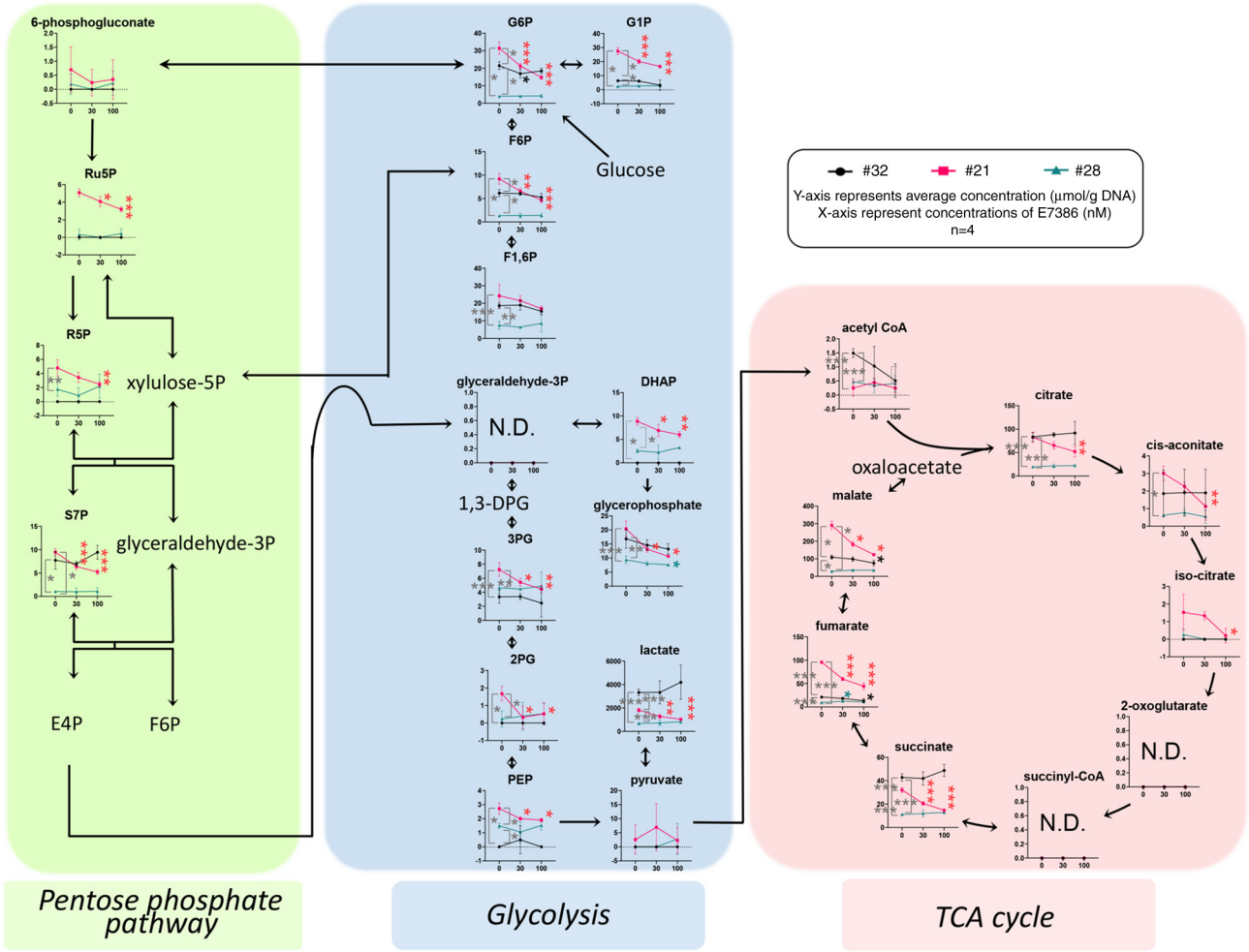

Figure 4. Quantified levels of metabolites produced by the pentose phosphate pathway, glycolysis and TCA cycle after treatment with E7386 in CRC organoids. Quantified levels of metabolites involved in central carbon metabolism. Average metabolite concentrations (nmol/g DNA) in organoids treated with E7386 at concentrations of 0, 30 and 100 nM superimposed onto a metabolic pathway map. Pathways included glycolysis, pentose phosphate and the Kreb's cycle pathways. *P<0.05, **P<0.01 and ***P<0.001. The color of asterisks represents significance compared to the corresponding 0 nM controls in case 21 (red), case 28 (green) or case 32 (black). Data are presented as the mean ± SD. N.D., the metabolite concentration was below the detection limit of the analysis; TCA, tricarboxylic acid; CRC, colorectal cancer.

the subcutis of NOG mice, followed by confirmation of their engraftment, were used. No obvious changes after the administration of E7386 could be found in the size of tumor tissues (Figs. S5 and S6) or histopathological characteristics of PDX from cases 21 and 28 (data not shown). Evaluation could not be performed in case 32. Immunohistochemistry staining for PCK2 revealed an increased tendency for cytoplasmic granular positivity in the carcinoma cells of case 21 in the E7386 group (Fig. 5A), which was confirmed by immunoblotting (Figs. S7A and S8A), but not in case 28 (Figs. S7D and S8A). No clear changes in PCK2 positivity could be observed between the E7386 and control groups from cases 28 and 32 (Table SVI). VLDLR staining could be detected on the apical surface of the carcinoma cells in the control and E7386 groups of cases 21 and 28. However, in case 32, they were strongly visible not only on the apical surface but also on the intercellular membranes in the E7386 group (P=0.014; Fig. 5B; Table SVI). In terms of β-catenin, nuclear positivity in the carcinoma cells of case 28 tended to decrease in the E7386 group compared with that in the control group (Fig. 3C) but not in cases 21 and 32 (Table SVI). According to β-catenin immunoblotting, no notable changes in expression could be observed between the E7386 and control groups in cases 21 and 28 (Figs. S7B, S7E and S8B). As a marker for the activation of CAFs, immunohistochemistry staining for αSMA was performed. αSMA expression in the CAFs surrounding the CRC foci in the E7386 group from cases 21 or 28 showed a tendency to decrease compared with that in the control group (Figs. 5D and S9; Table SVI). The visually judged data was not necessarily reflected to the quantitative data.

Discussion

In the present study, the following were found: i) E7386 inhibited the viability of both CRC organoids and CAFs; ii) upregulation of genes associated with gluconeogenesis and cellular amino acid metabolism in the both organoids and CAFs following E7386 treatment were found; iii) hydrophilic metabolomic analysis in the organoid samples revealed the depletion of glycolytic metabolites after E7386 treatment; and iv) in the PDX model, membranous positivity for VLDLR and nuclear positivity for β-catenin in carcinoma cells were increased, but

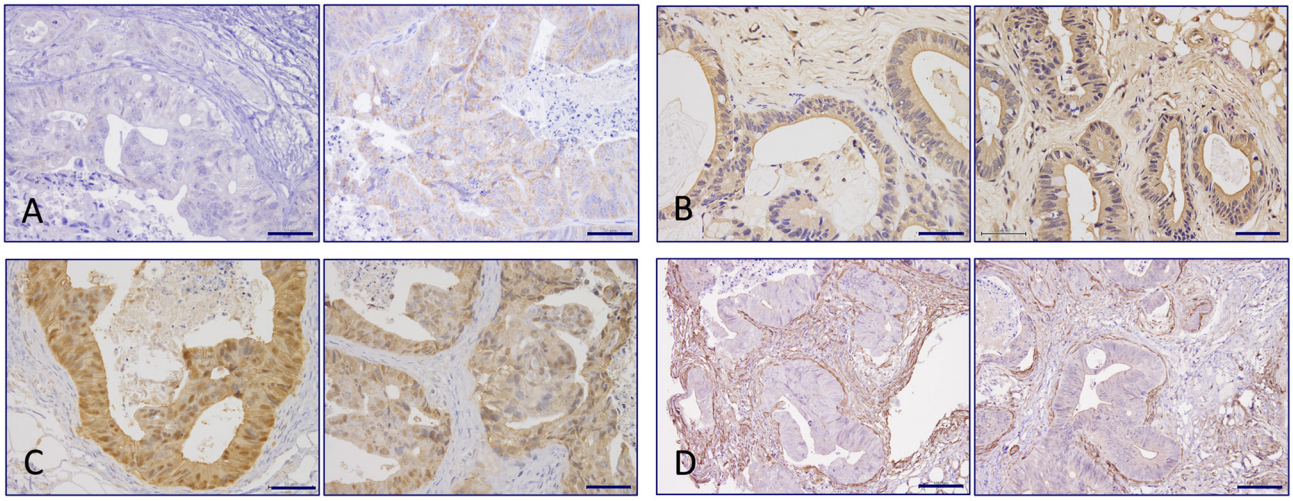

Figure 5. Results in the *in vitro* experiments are partially supported on the protein expression level in PDX models. Immunohistochemistry staining for (A) phosphoenolpyruvate carboxykinase 2 from case 21, (B) very low density lipoprotein receptor from case 32, (C) β-catenin from case 28 and (D) α-smooth muscle actin from case 28. The left panel represents PDXs treated with E7380 at 0 mg/kg, whereas the right panel represents PDXs treated with E7380 at 50 mg/kg bodyweight, twice a day for 14 days. Scale bars, 50 μm. PDX, patient-derived xenografts.

in turn showed a tendency to decrease after E7386 treatment, in of one of three cases. By contrast, the expression of αSMA in CAFs showed a tendency to decrease in two of the three cases after E7386 treatment. In addition, it was noteworthy that in organoids, the expression of genes associated with stress responses and NK-cell mediated cytotoxicity were also increased. By contrast, in CAFs *ACTA2*/αSMA expression were partially decreased.

The Wnt/β-catenin signaling pathway has been widely reported to regulate the expression of target genes downstream, primarily those associated with cell proliferation and differentiation (22). Furthermore, the Wnt signaling pathway has been documented to serve an important role in the activation of not only CRC cells but also CAFs (8). Therefore, E7386, a selective inhibitor of the interaction between β-catenin and the CREB binding protein, was hypothesized to exert a physiological effect on CRC cells. This was likely particularly in those with constitutively active Wnt/β-catenin signaling but without mutations in the driver oncogenes of key signaling pathways. Inhibitory effects on the viability of organoids were observed after treatment with 100 nM E7386, which was more potent in the co-cultured groups of cases 21 (harboring *APC*, *KRAS* and *TP53* mutations) and 32 (harboring *APC* and *TP53* mutations). However, the effects of E3786 were diminished in the single-culture groups of case 21. In case 28, which harbored *PIK3CA* and *TP53* mutations, inhibitory effects of E7386 on the viability of organoids were observed at 300 nM. The inhibitory effects of E7386 on CAF viability were also observed at 100 nM, which were more potent in the single-culture group from the three cases. These results suggest that E7386 affected not only the CRC organoids but can also the CAFs differently depending on each individual case. There was a report supporting the present results, where CAFs derived from CRC tissues revealed a differential transcriptomic profile compared with that in fibroblasts derived from the paired adjacent normal mucosal tissue of each case (8). Wnt signaling, focal adhesion and cell cycle progression were proposed to be involved (8). The effect of E7386 on the viability of organoids and CAFs was evaluated according to the minimum inhibitory concentrations (MIC), not IC_{50}, since organoids/CAFs with low response rates were found among the cases in the present experiment.

To clarify the molecular events underlying the inhibitory effects of E7386 on CRC organoids and CAFs, a DNA microarray analysis was performed. No obvious changes in the direct target genes of Wnt signaling pathway were observed in the present experiments. The cause of these results could be that E7386 is a selective inhibitor of the interaction between β-catenin and the CREB binding protein, whilst not being a direct inhibitor of β-catenin. One of the main findings was that the number of upregulated and downregulated genes in CAFs associated E7386 concentrations was higher (458 and 431, respectively), compared with those (46 and 17, respectively) in organoids, suggesting that E7386 can exert effects on not only in CRC organoids but also in CAFs. The upregulated genes in CAFs at 100 nM included those in cellular amino acid metabolism and gluconeogenesis, suggesting that the inhibition of CAF viability was partly associated with the disruption of glucose and amino acid metabolism. Furthermore, *DIAPH1*, which was previously reported to be associated with the differentiation of hepatic stellate cells into tumor-promoting myofibroblasts (21), was decreased after E7386 treatment. The expression levels of *ACTA2*/αSMA, which indicates the general phenotype of CAFs, were also found to be decreased on both gene and protein expression levels after treatment with E7386, suggesting that E7386 inhibited the activation of CAFs.

Among the genes in the glucose and amino acid metabolic pathways, the expression of *ASNS*, *PSAT1*, *PHGDH* and *PCK2* were increased in organoids after treatment with 100 nM E7386, which also decreased cell viability. Hydrophilic metabolomic analysis of E7386-treated organoids revealed the depletion of glucose, essential and several non-essential amino acids, which supported the transcriptomic data, particularly in case 21. In the tumor environment, metabolic adaptations can occur, which may reflect the survival responses of not only cancer cells but also the surrounding fibroblasts (23,24). These

adaptations include metabolite sharing and nutrient competition (23,24).

In addition to those directly related to glucose and amino acid metabolism, upregulation of *CHAC1* expression in organoids by E7386 was suggested to act by the pharmacological inhibition of antiporter system X_c^-, resulting in cystine-glutamate exchange and the induction of endoplasmic reticulum stress and ferroptosis (25). Upregulation of *ULBP1* expression suggested that E7386 may activate natural killer group 2, member D (*NKG2D*). It has been extensively reported that induction of the NKG2D ligands, ULBP1-6 and major histocompatibility complex class I chain-related genes A/B), can enhance NK cell recognition of cancer cells to mediate the lysis of the latter (26).

E7386 suppresses the β-catenin/cAMP-binding protein axis by inhibiting their interaction without affecting the β-catenin/p300 complex (10). Therefore, E7386 was considered to function as a Wnt signaling modulator (10). The precise molecular mechanisms underlying the E7386-induced phenotypes remain poorly understood. Wnt signaling activity is closely associated with glucose level in tumor cells, such that glucose can promote the formation of the lymphoid enhancer binding factor 1 (LEF1)/β-catenin complex, leading to β-catenin acetylation and increased transcriptional activity (27). The close interaction among the signals related to LEF1/β-catenin-driven gene expression changes raises the possibility of a positive feedback loop, where Wnt suppression may cause alterations in glucose metabolism. β-catenin has been reported to serve a role in NK T-cell development and function (28). A recent study showed that suppression of β-catenin activity by ICG-001, an inhibitor of the interaction between cAMP-binding protein and β-catenin, enhanced the early IFN-γ responses of NKT cells stimulated with a-galactosylceramide (29). These results suggest that upregulation of ULBP1 may be involved in the activation.

To confirm the transcriptomic data found after the *in vitro* experiments, immunohistochemical staining analysis was performed using E7386-treated PDX models. PCK2-positivity in the CRC cells was increased in the E7386-treated PDX group from case 21, which was consistent with results from immunoblotting analysis. However, PCK2 protein expression levels remained unchanged in cases 32 and 28. In the hydrophilic metabolomic analysis of the *in vitro* experiments, the concentrations of G6P and G1P in the control of case 21 were higher compared with those of cases 32 and 28, whereas those of case 21 were decreased by treatment with E7386. This suggested that E7386 treatment induced glucose depletion. The cause of this higher potency of E7386 on glucose metabolism in case 21 warrants further investigation. Enhancement of immunoreactivity to VLDLR in E7386-administered PDXs from case 32 was consistent with the DNA microarray data. VLDLR is a multifunctional receptor that regulates cellular signaling by binding numerous ligands. Its expression has been reported to be downregulated in CRC tissues compared with that in their corresponding paired adjacent non-tumor tissues. Additionally, VLDLR overexpression has been shown to inhibit the proliferation and migration of CRC cells (30). VLDLR was proposed to mediate effects on the Wnt/β-catenin signaling pathway (31). Although changes in the expression of β-catenin on both gene and protein levels could not be detected in the present study, a tendency for its reduction in the nucleus according to immunohistochemical staining was observed in the E7386-administered PDXs from case 28. There is a possibility that the β-catenin-negative regions in the nucleus were predominantly grown by E7386 administration in PDXs. To verify the transcriptomic data obtained in the *in vitro* experiments using CAFs, immunohistochemical staining for αSMA using PDX models was conducted. αSMA expression in the fibroblasts surrounding the CRC cell foci in the E7386-administered groups from cases 28 and 21 showed a tendency to decrease compared with that in the corresponding control group. This was consistent with the transcriptomic data.

In conclusion, the present comprehensive molecular analysis of E7386-treated CRC organoids, CAFs and PDXs revealed that several independent molecular mechanisms may be involved upstream of the reduction of cell viability. Alterations in the expression of genes associated with the glucose and amino acid metabolic pathways, namely PCK2, ASNS, PSAT1 and PHGDH, were observed. In addition, genes related to the stimulation of stress responses and NK-cell mediated cytotoxicity, specifically CHAC1 and ULBP1, were found to be altered. Modifications in the expression and localization of components in the Wnt/β-catenin signaling pathway, VLDLR and β-catenin, were also found. Further studies using preclinical models are required to clarify the molecular mechanisms underlying the E7386-induced reactions, with focus on the Wnt/β-catenin signaling pathway. Furthermore, association studies and analyses between preclinical data and clinical sample-based biomarker need to be performed to evaluate the accuracy of the preclinical models used in the present study.

Acknowledgements

The authors would like to thank Ms Yurika Shiotani (The Omics Core and Animal Core Facilities of the National Cancer Center Research Institute, Tokyo, Japan) for her technical support in histopathological evaluation. In addition, the authors would like to thank Mr Ryoichi Masui and Ms Ruri Nakanishi (Central Animal Division, National Cancer Center Research Institute, Tokyo, Japan) for their technical assistance.

Funding

The present study was supported by a grant for Research on Development of New Drugs (Funding for Research to Expedite Effective Drug Discovery by Government, Academia and Private Partnership; grant no. JP19ak0101043h0105) from the Japan Agency for Medical Research and Development. The core facilities were supported by the National Cancer Center Research and Development Fund (grant no. 2020-J-002).

Availability of data and materials

The datasets presented in this study can be found in online repositories. The names of the repository/repositories and accession number(s) can be found below: DDBJ database: https://ddbj.nig.ac.jp/public/ddbj_database/gea/experiment/E-GEAD-000/E-GEAD-492 (GEA accession number, E-GEAD-492).

Authors' contributions

MO, SI, MK and YK performed the experiments. MN, KM, AH, TS, YH and AY contributed to the analysis and interpretation of data. AO conceptualized the study. TI was responsible for the study design and data analysis. All authors confirm the authenticity of the raw data and have read and approved the final manuscript.

Ethics approval and consent to participate

The use of surgical specimens in this study was approved by the Ethics Committee of the National Cancer Center (approval no. 2015-108) and written informed consent was obtained from all patients. Ethics approval was obtained from the National Cancer Center Animal Ethics Committee (approval no. T17-006) for the animal studies.

Patient consent for publication

Not applicable.

Competing interests

YH and AY report personal fees from Eisai Co., Ltd. for the duration of the present study and outside of the present submitted work. The other authors declare that they have no competing interests.

References

1. Dekker E, Tanis PJ, Vleugels JL, Kasi PM and Wallace MB: Colorectal cancer. Lancet 394: 1467-1480, 2019.
2. Siegel RL, Miller KD, Goding Sauer A, Fedewa SA, Butterly LF, Anderson JC, Cercek A, Smith RA and Jemal A: Colorectal cancer statistics, 2020. CA Cancer J Clin 70: 145-164, 2020.
3. Fearon ER and Vogelstein B: A genetic model for colorectal tumorigenesis. Cell 61: 759-767, 1990.
4. Burrell RA, McGranahan N, Bartek J and Swanton C: The causes and consequences of genetic heterogeneity in cancer evolution. Nature 501: 338-345, 2013.
5. Normanno N, Rachiglio AM, Lambiase M, Martinelli E, Fenizia F, Esposito C, Roma C, Troiani T, Rizzi D, Tatangelo F, *et al*: Heterogeneity of KRAS, NRAS, BRAF and PIK3CA mutations in metastatic colorectal cancer and potential effects on therapy in the CAPRI GOIM trial. Ann Oncol 26: 1710-1714, 2015.
6. Kim TM, Lee SH and Chung YJ: Clinical applications of next-generation sequencing in colorectal cancers. World J Gastroenterol 19: 6784-6793, 2013.
7. Cancer Genome Atlas Network: Comprehensive molecular characterization of human colon and rectal cancer. Nature 487: 330-337, 2012.
8. Berdiel-Acer M, Sanz-Pamplona R, Calon A, Cuadras D, Berenguer A, Sanjuan X, Paules MJ, Salazar R, Moreno V, Batlle E, *et al*: Differences between CAFs and their paired NCF from adjacent colonic mucosa reveal functional heterogeneity of CAFs, providing prognostic information. Mol Oncol 8: 1290-1305, 2014.
9. Naruse M, Ochiai M, Sekine S, Taniguchi H, Yoshida T, Ichikawa H, Sakamoto H, Kubo T, Matsumoto K, Ochiai A and Imai T: Re-expression of REG family and DUOXs genes in CRC organoids by co-culturing with CAFs. Sci Rep 11: 2077, 2021.
10. Yamada K, Hori Y, Inoue S, Yamamoto Y, Iso K, Kamiyama H, Yamaguchi A, Kimura T, Uesugi M, Ito J, *et al*: E7386, a selective inhibitor of the interaction between beta-catenin and CBP, exerts antitumor activity in tumor models with activated canonical Wnt signaling. Cancer Res 81: 1052-1062, 2021.
11. Livak KJ and Schmittgen TD: Analysis of relative gene expression data using real-time quantitative PCR and the 2(-Delta Delta C(T)) method. Methods 25: 402-408, 2001.
12. Zhou Y, Zhou B, Pache L, Chang M, Khodabakhshi AH, Tanaseichuk O, Benner C and Chanda SK: Metascape provides a biologist-oriented resource for the analysis of systems-level datasets. Nat Commun 10: 1523, 2019.
13. Soga T, Baran R, Suematsu M, Ueno Y, Ikeda S, Sakurakawa T, Kakazu Y, Ishikawa T, Robert M, Nishioka T and Tomita M: Differential metabolomics reveals ophthalmic acid as an oxidative stress biomarker indicating hepatic glutathione consumption. J Biol Chem 281: 16768-16776, 2006.
14. Hirayama A, Kami K, Sugimoto M, Sugawara M, Toki N, Onozuka H, Kinoshita T, Saito N, Ochiai A, Tomita M, *et al*: Quantitative metabolome profiling of colon and stomach cancer microenvironment by capillary electrophoresis time-of-flight mass spectrometry. Cancer Res 69: 4918-4925, 2009.
15. Naruse M, Ishigamori R and Imai T: The unique genetic and histological characteristics of DMBA-induced mammary tumors in an organoid-based carcinogenesis model. Front Genet 12: 768731, 2021.
16. Kanda Y: Investigation of the freely available easy-to-use software 'EZR' for medical statistics. Bone Marrow Transplant 48: 452-458, 2013.
17. Bae JH, Kim SJ, Kim MJ, Oh SO, Chung JS, Kim SH and Kang CD: Susceptibility to natural killer cell-mediated lysis of colon cancer cells is enhanced by treatment with epidermal growth factor receptor inhibitors through UL16-binding protein-1 induction. Cancer Sci 103: 7-16, 2012.
18. Vincent EE, Sergushichev A, Griss T, Gingras MC, Samborska B, Ntimbane T, Coelho PP, Blagih J, Raissi TC, Choiniere L, *et al*: Mitochondrial phosphoenolpyruvate carboxykinase regulates metabolic adaptation and enables glucose-independent tumor growth. Mol Cell 60: 195-207, 2015.
19. Arce L, Pate KT and Waterman ML: Groucho binds two conserved regions of LEF-1 for HDAC-dependent repression. BMC Cancer 9: 159, 2009.
20. Chen Z, Chen G and Zhao H: FDPS promotes glioma growth and macrophage recruitment by regulating CCL20 via Wnt/β-catenin signalling pathway. J Cell Mol Med 24: 9055-9066, 2020.
21. Liu D, Fu X, Wang Y, Wang X, Wang H, Wen J and Kang N: Protein diaphanous homolog 1 (Diaph1) promotes myofibroblastic activation of hepatic stellate cells by regulating Rab5a activity and TGFβ receptor endocytosis. FASEB J 34: 7345-7359, 2020.
22. Clevers H and Nusse R: Wnt/β-catenin signaling and disease. Cell 149: 1192-1205, 2012.
23. Kalluri R: The biology and function of fibroblasts in cancer. Nat Rev Cancer 16: 582-598, 2016.
24. Lyssiotis CA and Kimmelman AC: Metabolic interactions in the tumor microenvironment. Trends Cell Biol 27: 863-875, 2017.
25. Dixon SJ, Patel DN, Welsch M, Skouta R, Lee ED, Hayano M, Thomas AG, Gleason CE, Tatonetti NP, Slusher BS and Stockbell BR: Pharmacological inhibition of cystine-glutamate exchange induces endoplasmic reticulum stress and ferroptosis. Elife 3: e02523, 2014.
26. Raulet DH, Gasser S, Gowen BG, Deng W and Jung H: Regulation of ligands for the NKG2D activating receptor. Annu Rev Immunol 31: 413-441, 2013.
27. Chocarro-Calvo A, Garcia-Martinez JM, Ardila-Gonzalez S, De la Vieja A and Garcia-Jimenez C: Glucose-induced β-catenin acetylation enhances Wnt signaling in cancer. Mol Cell 49: 474-486, 2013.
28. Kling JC and Blumenthal A: Roles of WNT, NOTCH, and Hedgehog signaling in the differentiation and function of innate and innate-like lymphocytes. J Leukoc Biol 101: 827-840, 2017.
29. Kling JC, Jordan MA, Pitt LA, Meiners J, Thanh-Tran T, Tran LS, Nguyen TT, Mittal D, Villani R, Steptoe RJ, *et al*: Temporal regulation of natural killer T Cell interferon gamma responses by beta-catenin-dependent and -independent Wnt signaling. Front Immunol 9: 483, 2018.
30. Kim BK, Yoo HI, Lee AR, Choi K and Yoon SK: Decreased expression of VLDLR is inversely correlated with miR-200c in human colorectal cancer. Mol Carcinog 56: 1620-1629, 2017.
31. Lee K, Shin Y, Cheng R, Park K, Hu Y, McBride J, He X, Takahashi Y and Ma JX: Receptor heterodimerization as a novel mechanism for the regulation of Wnt/β-catenin signaling. J Cell Sci 127: 4857-4869, 2014.